Journal of Physics D: Applied Physics

PAPER

Generalized perfect optical vortices along arbitrary trajectories

To cite this article: Yue Chen *et al* 2021 *J. Phys. D: Appl. Phys.* **54** 214001

IOP Publishing Journal of Physics D: Applied Physics
J. Phys. D: Appl. Phys. **54** (2021) 214001 (7pp) https://doi.org/10.1088/1361-6463/abe66b

Generalized perfect optical vortices along arbitrary trajectories

Yue Chen[1], Tingchang Wang[2], Yuxuan Ren[3], Zhaoxiang Fang[4], Guangrui Ding[2], Liqun He[5], Rongde Lu[6,*] and Kun Huang[4,*]

[1] Department of Engineering and Applied Physics, University of Science and Technology of China, Hefei 230026, People's Republic of China
[2] School of the Gifted Young, University of Science and Technology of China, Hefei 230026, People's Republic of China
[3] Department of Electrical and Electronic Engineering, University of Hong Kong, Pokfulam Road, Hong Kong, People's Republic of China
[4] Department of Optics and Optical Engineering, University of Science and Technology of China, Hefei 230026, People's Republic of China
[5] Department of Thermal Science and Energy Engineering, University of Science and Technology of China, Hefei 230026, People's Republic of China
[6] Physics Experiment Teaching Center, University of Science and Technology of China, Hefei 230026, People's Republic of China

E-mail: lrd@ustc.edu.cn and huangk17@ustc.edu.cn

Received 30 November 2020, revised 31 January 2021
Accepted for publication 15 February 2021
Published 3 March 2021

Abstract

Perfect optical vortices (POVs) arevortex beams with infinitely narrow rings and fixed radii independent of their topological charges. Here we propose the concept of generalized POVs (GPOVs) along arbitrary curves beyond the regular shapes of circles and ellipses. GPOVs share similar properties to POVs, such as defined only along infinitely narrow curves and owning topological charges independent of scale. Using a rigorous mathematical derivation in a curvilinear coordinate, we reveal theoretically that the GPOVs have a topological charge proportional to the area of the swept sector in tracing the curve, suggesting a unique mode for optical vortex beams. Experimentally, the complex-amplitude masks to generate the GPOVs are realized by using a pure-amplitude digital micro-mirror device with the super-pixel encoding technique. The phase profiles of the generated GPOVs are retrieved experimentally through self-built interferometry and exhibit good agreement with the simulations. We also derive a properly modified formula to yield the intensity-uniform GPOVs along predesigned curves, which might find applications in optical tweezers and communications.

Keywords: structured light, perfect vortex, wavefront shaping

(Some figures may appear in colour only in the online journal)

1. Introduction

Optical vortices (OVs) with helical wavefronts carry orbital angular momentum (OAM) [1] of $l\hbar$ per photon (l is the topological charge and $\hbar$ is the reduced Planck constant), recognized by Allen *et al* [2]. The pioneering work has excited intense research on OVs in various applications including manipulation of microparticles [3–10], optical communication [11, 12], quantum information [13–15], plasma diagnostics [16–18], optical imaging and probing [19], and plasmonics [20, 21]. Among these applications, the widely used vortex beams, such as Laguerre–Gaussian beams and Bessel beams, have the radii of their annular rings determined by their topological charges. As a topological invariant, the topological charge is the most important factor protecting the radial structure of an OV beam from environmental disturbances, which is known as the self-healing effect [22, 23]. Such a topologically

* Authors to whom any correspondence should be addressed.

dependent intensity profile exists in all the optical vortex beams and thus leads to inconveniences when working in a limited field of view, e.g. the tight focusing case when using an objective lens with a high numerical aperture.

To overcome this disadvantage, a special type of OV, termed as the perfect OV (POV), was proposed in 2013 [24]. POVs have infinitely narrow rings with radii of r_0 which have nothing to do with the topological charges l. A POV can be described mathematically as $\delta(r-r_0)\exp(\mathrm{i}l\theta)$, where (r,θ) is the polar coordinate and $\delta(\cdot)$ is the Dirac delta function. Thus, one can separately control the phase and intensity structures of the OVs. By using diffractive optical elements [25], spatial light modulator [24], digital micro-mirror device (DMD) [26], some fruitful progress such as vector [27] and quantum [13] POVs have been achieved, facilitating applications in optical tweezers [28], non-diverging speckles [29] and optical free-space communication [11]. Very recently, the circular shape of POVs has been extended to the elliptical case by employing the Fraunhofer diffraction of elliptic Bessel beams [30]. This approach offers insight towards generalizing POVs with non-circular or arbitrary shapes with the help of optical Fourier transforms. The importance of arbitrarily curved POVs is twofold: for applications such as optical manipulation, these arbitrarily curved POVs enable the dynamic control of microparticles by using a single-shot beam thus avoiding the scanning mode in traditional trapping strategies; on the other hand, since several types of POVs have been reported in theory, a general analytical formula for POVs with predesigned shapes is highly demanded. There are two fundamental challenges to obtain such generalized POVs. Firstly, generalized POVs should be predesigned with infinitesimal width along arbitrary smooth trajectories. Secondly, the topological charges and local phase gradient of generalized POVs must be freely controlled.

In this letter, we propose theoretically and demonstrate experimentally generalized POVs (GPOVs) along arbitrary trajectories beyond the regular shapes of circles and ellipses. To realize the GPOVs experimentally, the required intensity and phase profiles are simultaneously encoded on a DMD as binary holograms, showcasing the GPOVs with circular, elliptic, asteroid, Archimedean spiral and 'elephant' trajectories. Moreover, we give a modified formula of GPOVs to obtain uniformly distributed trajectories in both theory and experiments.

2. Theory and simulation of GPOVs

2.1. Definition of GPOVs

We define GPOVs as arbitrarily curved POV beams whose intensity profiles obey the Dirac delta function along any customized trajectories and are independent of their topological charges. We consider a smooth 2D curve in Cartesian coordinates $\vec{c}_2(t)=(x_0(t),y_0(t)),t\in[0,T]$, where T is the maximum value of the parameter t. Note that the curve $\vec{c}_2(t)$ is independent of the coordinate transform, implying that the curve is invariant in all coordinates. Thus, it allows us to choose a suitable coordinate system to simplify the mathematical description of the GPOV. To describe the curve in a nonparametric form similar to the case in POVs ($\delta(r-r_0)\exp(il\theta)$, where (r,θ) is the polar coordinate) and elliptic POVs, we employ a specially designed spatial transform:

$$\begin{cases} x=px_0(q) \\ y=py_0(q) \end{cases}, \tag{1}$$

where (p,q) are the indices of a curvilinear coordinate system. To permit an inverse transformation, we also set the Jacobian determinant $|J(p,q)|$ of the conversion to be non-zero:

$$|J(p,q)|=p\left[x_0(q)y'_0(q)-y_0(q)x'_0(q)\right]\neq 0. \tag{2}$$

In this curvilinear coordinate system (p,q), $\vec{c}_2(t)$ can be written as $p=1$. Thus, the GPOV amplitude along the given curve can be written as an invariant form: $\delta(p-1)$. Then, we focus on the definition of the spiral phase term of the GPOV. The phase term determined by the given curve should also be invariant under various coordinate transforms. Considering that the phase is spirally surrounding the singular center, we define the spiral phase to be proportional to the oriented area of the swept sector along the curves: $\frac{1}{2}\int_0^q|J(1,\tau)|\,\mathrm{d}\tau$, where τ is the integral variable. Now we come up with the exact mathematical formula of GPOVs satisfying the definition of GPOVs mentioned above:

$$C(x,y,z=0\,|\vec{c}_2(t),t\in[0,T])=\delta(p(x,y)-1)\times\exp\left[\mathrm{i}\sigma\int_0^{q(x,y)}|J(1,\tau)|\,\mathrm{d}\tau\right], \tag{3}$$

where $(p(x,y),q(x,y))$ is the position vector at the curvilinear coordinate plane defined in equation (1), σ is the key parameter controlling the local phase gradient and topological charges of GPOVs along the curves and $C(\cdot)$ is the complex amplitude of GPOVs in spatial domain. The Dirac delta function indicates that GPOVs own infinitely narrow profiles along given curves. The phase term is represented in terms of a curve invariant proportional to the oriented area of the sector swept in tracing the curves, which means the beams are defined by the curves as geometric objects at the plane ($z=0$). The infinitesimal width (defined by delta function) and the controllable local phase gradient make our GPOVs distinguished fundamentally from the previous vortices with arbitrary trajectories [31, 32].

The optical angular momenta of GPOVs are related to their topological charges, which are extremely important to investigate OVs in both theory and applications. We also calculate the total topological charges l of the GPOVs:

$$l(x,y\,|\vec{c}_2(t),t\in[0,T])=\frac{\sigma}{2\pi}\int_0^T|J(1,\tau)|\,\mathrm{d}\tau. \tag{4}$$

The integrated term in equation (4) is also a curve invariant defined as a geometric object which is consistent with the invariance of the topological charges. Therefore, equation

(4) reveals that the topological charge of GPOVs is proportional to the oriented area of the sector swept in tracing the curves, which is also an invariable. In addition, the local phase gradient $(\nabla\phi(x,y)=\sigma|J(1,q(x,y))|\nabla q(x,y))$ and topological charges of GPOVs can be freely controlled by the parameter σ, which is independent of their intensity scales.

Next, we exemplify a type of GPOV along elliptic curves $\vec{c}_2(t)=(a\cos t, b\sin t), t\in[0,2\pi]$, where a,b are the semi-major axis and semi-minor axis of ellipses. By using the coordinate transform in equation (1), the elliptic GPOVs have the form:

$$C(x,y,z=0|\text{Ellipse})=\delta(p-1)\exp(\mathrm{i}\sigma abq), \tag{5}$$

where $p=\sqrt{\frac{x^2}{a^2}+\frac{y^2}{b^2}}$, $q=\arg(bx+\mathrm{i}ay)$. We can rewrite equation (5) in a familiar form:

$$C(x,y,z=0|\text{Ellipse})=r_0\delta(r-r_0)\exp(\mathrm{i}l\theta), ss \tag{6}$$

where $r=\sqrt{\frac{b}{a}x^2+\frac{a}{b}y^2}, \theta=\arg(bx+\mathrm{i}ay), r_0=\sqrt{ab}, l=\sigma ab$. Equation (6) is the exact expression of an elliptic perfect vortex (EPOV) [33]. Thus, we have proved that EPOVs are just GPOVs along elliptic curves. It therefore confirms the validity of the concept of GPOVs.

2.2. GPOVs in frequency domain

Due to the infinitely narrow intensity profiles along curves and complex expression of GPOVs in spatial domain, it is a common approach to investigate them in a frequency domain similar to POVs and EPOVs [30, 33, 34]. In a practical setup, the GPOVs in the frequency domain are placed at the initial plane. After passing through a Fourier lens with focal length of f, the GPOVs in the spatial domain are generated at the Fourier plane. Therefore, we can derive the complex amplitude of GPOVs in the frequency domain through an optical inverse Fourier transform:

$$Y(x_1,y_1|\vec{c}_2(t),t\in[0,T])=\frac{1}{\lambda f}\iint_{R^2}C(x,y,z=0)\times\exp\left[\mathrm{i}\frac{2\pi}{\lambda f}(x_1x+y_1y)\right]\mathrm{d}x\mathrm{d}y, \tag{7}$$

where (x_1,y_1) is the position vector at the initial plane, (x,y) is the position vector at the Fourier plane, λ is the wavelength of the beams and $Y(\cdot)$ is the complex amplitude of GPOVs in the frequency domain. After substituting equation (3) into equation (7), the complex amplitude of GPOVs in frequency domain can be simplified further:

$$Y(x_1,y_1|\vec{c}_2(t),t\in[0,T])=\frac{1}{\lambda f}\int_0^T\Phi_Y(x_1,y_1,t)|J(1,t)|\,\mathrm{d}t, \tag{8}$$

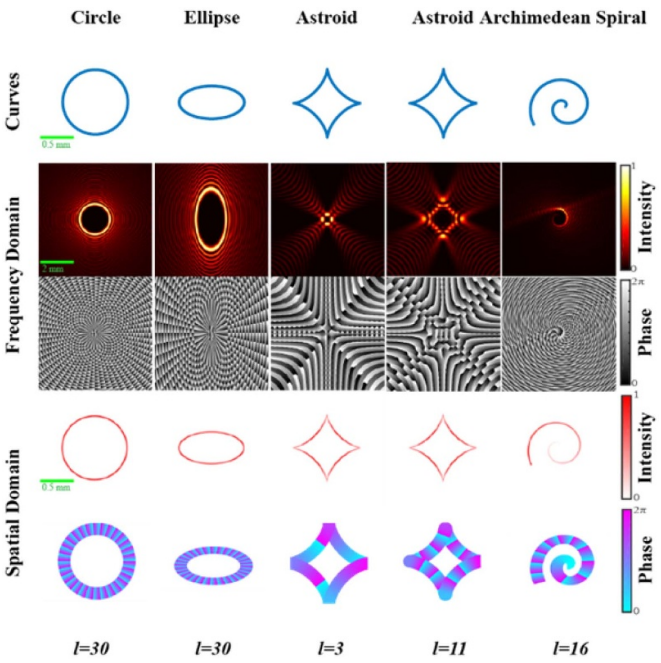

Figure 1. The normalized intensity and phase profiles of GPOVs in frequency domain (initial plane) and in spatial domain (Fourier plane) along several curves via simulations. The color bars and scale bars are shown.

where

$$\Phi_Y(x_1,y_1,t)=\exp\left[\mathrm{i}\frac{2\pi}{\lambda f}(x_1x_0(t)+y_1y_0(t))+\mathrm{i}\sigma\int_t^0|J(1,\tau)|\,\mathrm{d}\tau\right].$$

Note that this formula is expressed in Cartesian coordinates at the initial plane, which is easy to realize both in simulation and experiment.

2.3. Simulation method

According to the setup mentioned in section 2.2, Y is located at the initial plane and C is placed at Fourier plane of a lens. Firstly, we calculate the intensity and phase profiles of Y, which are shown in the second and third rows of figure 1. Notice that there are two integrals in equation (8), which requires additional attention in numerical simulation. Secondly, we calculate the Fourier transform of Y numerically, yielding C. The intensity and phase profiles of GPOVs are shown in the fourth and fifth rows of figure 1. The focal length of the Fourier lens is 200 mm and the laser wavelength is 632.8 nm in simulation. The simulation codes of GPOVs are implemented in MATLAB and publicly available (https://github.com/ChenYueWuDi/GPOVs.git.)

In addition to POVs and EPOVs, we also simulate two other types of GPOVs: the asteroid GPOV and Archimedean GPOV, as shown in figure 1. The corresponding formulas and parameters for the GPOVs in figure 1 are shown in table 1. These

Table 1. The formulas and parameters of the curves used in figure 1.

Curves $\vec{c}_2(t)$	Expressions	Parameters
Circle	$(R_0\cos t, R_0\sin t)$, $R_0 = 0.5\,\text{mm}$	$t \in [0, 2\pi]$; $\sigma = 1.2\times10^8\ \text{m}^{-2}$, $l = 30$
Ellipse	$(a\cos t,\ b\sin t)$ $a = 0.5\,\text{mm}$, $b = 0.25\,\text{mm}$	$t \in [0, 2\pi]$; $\sigma = 2.4\times10^8\ \text{m}^{-2}$, $l = 30$
Asteroid	$(3R_0\cos t + R_0\cos 3t,$ $3R_0\sin t - R_0\sin 3t)$ $R_0 = 0.15\,\text{mm}$	$t \in [0, 2\pi]$; $\sigma = 8.1\times10^7\ \text{m}^{-2}$, $l = 3$, $\sigma = 2.2\times10^7\ \text{m}^{-2}$, $l = 11$
Archimedean spiral	$(R_0 t\cos\omega t, R_0 t\sin\omega t)$, $R_0 = 0.5\,\text{mm}$, $\omega = 10$	$t \in [0, 1]$, $\sigma = 1.2\times10^8\ \text{m}^{-2}$, $l = 16$

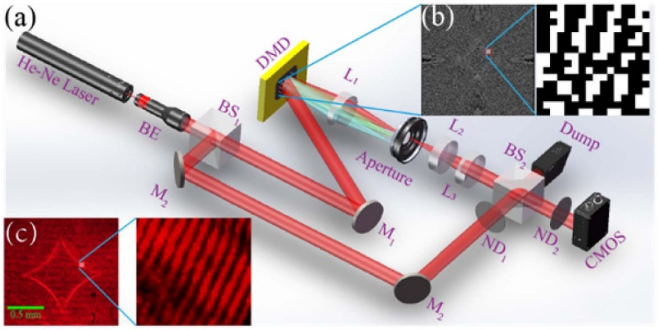

Figure 2. The experimental setup for beam generation and interferometry. (a) Optical setup; (b) binary hologram of asteroid GPOV ($l = 11$), inset is an enlarged view of the pattern; (c) interference pattern between an asteroid GPOV ($l = 11$) and a Gaussian beam. The insert is an enlarged view of the interferometric fringe.

GPOVs have extremely sharp intensity profiles along arbitrary curves $\vec{c}_2(t)$ with scales independent of topological charges. As an example, the asteroid GPOVs with topological charge of 3 (the third column in figure 1) and 11 (the fourth column in figure 1) possess exactly the same size at the coordinate space. Thus, we can customize the scales and topological charges separately. Additionally, the simulated Archimedean GPOV implies that our strategies are valid even for open curves, which could significantly extend the territory of POVs.

3. Experimental demonstration of GPOVs

3.1. Optical configuration

To demonstrate the proposed GPOVs experimentally, we build the 6 f beam generation setup (figure 2(a)) by using a DMD (DLP Discovery 4100, Texas Instruments, 1024 × 768). The He–Ne laser (HRS015B, Thorlabs, 632.8 nm) is collimated through a beam expander (BE, ×10) and a mirror M_1 to illuminate the DMD. A lens L_1 ($f_1 = 200$ mm) is used to focus light reflected from the DMD into a pinhole aperture which selects the first-order diffraction. The first-order diffraction is projected by a telescope consisted of lenses L_2 and L_3 ($f_2 = f_3 = 50\,\text{mm}$) onto a CMOS camera after passing through a neutral density ND_2 filter. An optical dump is used to collect undesired background light. By projecting the binary holograms onto the DMD, we could create steady GPOVs at the CMOS plane ($z = 0$).

3.2. Super-pixel method for holograms

To encode the complex field on DMD, the holograms created through the super-pixel method ares used to achieve full control over the spatial phase and amplitude [35, 36]. Such a configuration has sufficiently high resolution for encoding binary holograms compared with other binary methods. In a typical 4 f configuration, the super-pixel method generates binary holograms suitable for DMD. The DMD pixels at the input plane (the front focal plane of the first lens) are divided into several super-pixels and the prefactors for each pixels with one super-pixel are distributed uniformly between 0 and 2π. Thus, the total response at the output plane (the back focal plane of the second lens) is the summation of the individual pixel response. By programming the mask at the input plane, the required complex field can be realized at the output plane, where it is located at the coordinate space.

However, considering that the GPOVs have the shape of quite narrow curves with null intensity outside the curve region, we encode its complex field in frequency domain onto the DMD. Thus, we can obtain the curve shape directly at the Fourier plane of the lens L_1 by using the first-order diffraction, which is selected by a pinhole in our experiment. So, to record it, we need another confocal system (composed of the lenses L_2 and L_3) to project the curve (created at the Fourier plane of L_1) onto the back-focal plane of L_3, where the CMOS camera is located. Note that, the lenses L_2 and L_3 are confocal because the back focal plane of L_2 shares the same position with the front focal plane of L_3. In fact, the focal length of L_3 can be larger than that of L_2, so that the image of the curve is magnified for a better recording of intensity and the following interference experiment. The generated binary mask for the asteroid GPOV ($l = 11$) is exemplified in figure 2(b). The highlighted image of mask indicates the binary states of DMD pixels. Additionally, our generation codes of GPOVs are also publicly available at https://github.com/ChenYueWuDi/GPOVs.git.

3.3. Intensity and phase distribution of GPOVs in experiments

Figures 3(a)–(c) show the experimental intensity profiles of elliptic and asteroid GPOVs, respectively. The parameters are listed in table 1. The intensity profiles are very sharp along curves in all cases. Furthermore, the experiments of asteroid GPOVs with topological charges of $l = 3$ (figure 3(b)) and $l = 11$ (figure 3(c)) verify that the size of GPOVs are independent of their topological charges. The good agreement between simulated and measured intensity profiles implies the validity of the proposed GPOVs.

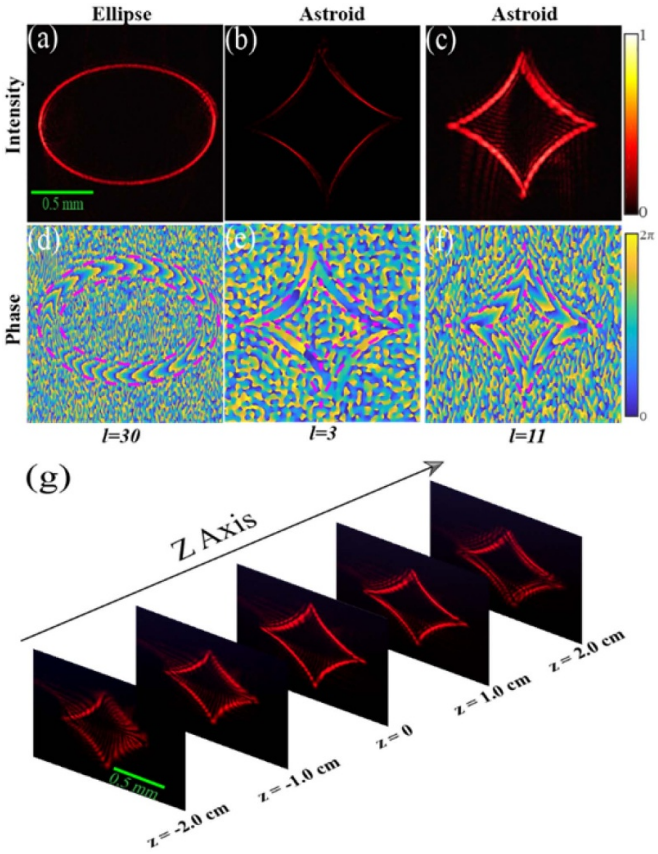

Figure 3. (a)–(f) The experimental intensity and phase distribution of GPOVs with elliptic and asteroid trajectories; (g) the intensity distribution of the GPOV ($l = 11$) with asteroid trajectory along z axis. The scale bars and color bars are shown.

To further measure the phase of the generated GPOVs, we apply a Mach–Zehnder interferometer to create the interference patterns between an asteroid GPOV ($l = 11$) and a Gaussian beam, as sketched in figure 2(a) [25, 37]. Two beam splitters (BS_1 and BS_2) are used to generate the object beams (GPOVs) and reference beams (Gaussian beams). The two beams are tuned into two co-propagating beams with a slightly oblique angle for generating the interference patterns and then recorded by the CMOS camera. In figure 2(c), we show the recorded interference pattern. The interference fringes for the case of the asteroid GPOV is shown in the enlarged insert image for better observation. Using the interference patterns, we could recover the exact phase profiles of GPOVs. Figures 3(d)–(f) show the experimentally recovered phase profiles of elliptic and asteroid GPOVs, respectively. The phase gradient along the curves within the purple dashed lines manifests that the generated GPOVs preserve the designed phase cycles of 30 (ellipse), 3 (asteroid) and 11 (asteroid). The twisted boundaries between phase cycles are caused by a defocus effect in experiments. Both experimental results agree well with the simulations. Furthermore, we also observe the propagation of the GPOVs, as shown in figure 3(g). The GPOVs are focused into extremely thin curves in the $z = 0$ plane. The intensity profiles deform at the out-of-focus planes due to the diffraction of light.

3.4. Modified formula for intensity-uniform GPOVs

Note that both the simulated and obtained intensity profiles are not uniform along the trajectories, except for circles. This inhomogeneous effect becomes severe especially at the cusp points along the curves, see the fourth row of figure 1 for example. This phenomenon originates from the unique properties of the Dirac delta function [38]. As shown in equation (3), the amplitude of GPOVs are defined as a nonparametric form $\delta(p-1)$ in a specially designed in a curvilinear coordinate system (p,q), where the amplitude of GPOVs are uniform. However, the GPOVs are usually expressed in Cartesian coordinates (x,y) as $\delta(p(x,y)-1)$ in both theory and experiments. The properties of delta function yield:

$$\delta(f(x,y)) = \begin{cases} \frac{1}{|\nabla f(x,y)|}, \text{ where } f(x,y)=0 \\ 0, \text{ where } f(x,y)\neq 0 \end{cases}. \tag{9}$$

Thus the amplitude of GPOVs along the curves where $f(x,y)=0$ is modulated by the ratio of the $|J(1,q(x,y))|$ term to $\left|\vec{c}_2'(q(x,y))\right|$ term, where $|\vec{c}'_2(q)| = \sqrt{x'^2_0(q)+y'^2_0(q)}$. Consider an elliptical GPOV for example, the modulation term is $\frac{ab}{\sqrt{(a^2-b^2)\sin^2\theta+b^2}}$. Thus the intensity a^2 occurs at $\theta=0$ and b^2 occurs at $\theta=\frac{\pi}{2}$, which can be identified at the first column of figures 1 and 3(a). This phenomenon has also been reported in EPOVs, where a properly designed elliptical aperture is suggested to realize a uniform amplitude distribution [30]. Unfortunately, it is quite difficult to design such apertures for other curves.

To further extend the potential applications of GPOVs, we generate GPOVs with uniform intensity along given curves. Here, we propose a modification on the expression of GPOVs as $C_{\text{Modified}}(\cdot)$, which can be treated as applying a predesigned amplitude modulation on GPOVs along the curves by the ratio of the $\left|\vec{c}_2'(q)\right|$ term to $|J(1,q)|$ term:

$$C_{\text{Modified}}(x,y,z=0|\vec{c}_2(t),t\in[0,T]) = \frac{|\vec{c}'_2(q)|}{J(1,q)}\delta(p-1) \times \exp\left[\mathrm{i}\sigma\int_0^q J(1,\tau)\,\mathrm{d}\tau\right]. \tag{10}$$

Similar to equation (7), we derive the predesigned amplitude modulation for GPOVs in frequency domain:

$$Y_{\text{Modified}}(x_1,y_1|\vec{c}_2(t),t\in[0,T]) = \frac{1}{\lambda f}\int_T^0 \Phi_Y(x_1,y_1,t)\,|\vec{c}'_2(t)|\,\mathrm{d}t. \tag{11}$$

The modified formulas equations (10) and (11) possess the same expression as the EPOVs with predesigned elliptical aperture in elliptic case. Furthermore, they can produce GPOVs with uniform intensity along other curves.

Figure 4 shows the simulated and experimental intensity distribution of GPOVs under the predesigned amplitude modulation described by equations (10) and (11). All the shapes including elliptical, asteroid ($l = 11$) and Archimedean curves (parameters are listed in table 1) can be realized experimentally, as shown in figures 4(e) and (g). In addition, an elephant

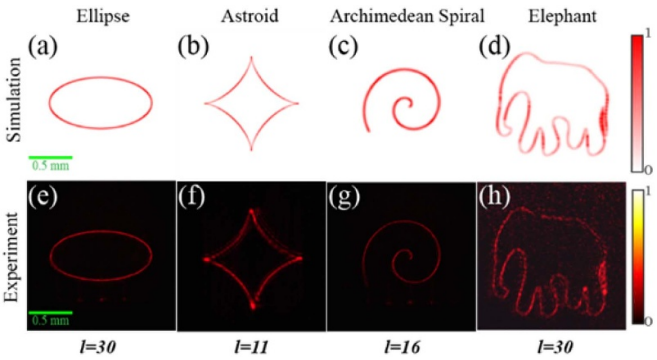

Figure 4. The simulated and experimental intensity distribution of modified GPOVs along several curves. The scale bars are shown.

curve with four feet and one nose is described mathematically with the help of a Fourier series, where $\sigma = 1.2 \times 10^8\,\mathrm{m}^{-2}$, $l = 30$. Such a GPOV with the elephant curve is experimentally generated with a continuous profile in figure 4(h), which is highly consistent with the simulation in figure 4(d). Compared with figure 1, the revised formula yields better uniformity for intensity profiles along the curves. By using this revision, we can overcome the key difficulties in applying the GPOVs in fields such as optical trapping and single shot lithography [39].

4. Conclusions

In conclusion, we have proposed the concept of GPOVs along arbitrary curves. GPOVs with various shapes possess similar properties as POVs, such as defined only along infinitely narrow curves and owning topological charges independent of scale. Note that they naturally degenerate to POVs and elliptic POVs in circle and ellipse cases, respectively. For applications such as optical trapping and single shot lithography, we give a properly modified formula of GPOVs to produce uniform intensity along predesigned curves. We also experimentally generate the GPOVs through a DMD and measure their phase profiles by interfering with Gaussian beams. The experimental results are consistent with the simulations. These vortex beams are valuable in micromanipulation, quantum communication, optical imaging, and single-shot lithography.

Acknowledgments

This work is sponsored by the National Natural Science Foundation of China (31670866, 60974038, 61875181, 61705085); Natural Science Foundation of Anhui Province (1708085MF143); CAS Pioneer Hundred Talents Program; USTC Research Funds of the Double First-Class Initiative (Grant No. YD2030002003). K H thanks the support from the University of Science and Technology of China's Centre for Micro and Nanoscale Research and Fabrication.

ORCID iDs

Yue Chen https://orcid.org/0000-0002-5619-6917
Yuxuan Ren https://orcid.org/0000-0002-4641-3148
Liqun He https://orcid.org/0000-0002-5857-0490
Kun Huang https://orcid.org/0000-0002-9391-149X

References

[1] Franke-Arnold S, Allen L and Padgett M 2008 *Laser Photon. Rev.* **2** 299–313
[2] Allen L, Beijersbergen M W, Spreeuw R J C and Woerdman J P 1992 *Phys. Rev.* A **45** 8185–9
[3] Padgett M and Bowman R 2011 *Nat. Photon.* **5** 343–8
[4] Guo C-S, Zhang Y, Han Y-J, Ding J-P and Wang H-T 2006 *Opt. Commun.* **259** 449–54
[5] Jesacher A, Maurer C, Schwaighofer A, Bernet S and Ritsch-Marte M 2008 *Opt. Express* **16** 4479–86
[6] Woerdemann M, Alpmann C, Esseling M and Denz C 2013 *Laser Photon. Rev.* **7** 839–54
[7] Wu J, Tang X and Xia J 2019 *Nanomaterials* **9** 87
[8] Rodrigo J A and Alieva T 2015 *Optica* **2** 812
[9] Gu F, Gu Z, Chang C, Yuan C, Feng S, Xing F and Nie S 2019 *IEEE Photon. J.* **11** 1–11
[10] Abramochkin E and Volostnikov V 2004 *Phys.-Usp.* **47** 1177–203
[11] Zhu F, Huang S, Shao W, Zhang J, Chen M, Zhang W and Zeng J 2017 *Opt. Commun.* **396** 50–7
[12] Gong L, Zhao Q, Zhang H, Hu X-Y, Huang K, Yang J-M and Li Y-M 2019 *Light Sci. Appl.* **8** 27
[13] Bozinovic N, Yue Y, Ren Y, Tur M, Kristensen P, Huang H, Willner A E and Ramachandran S J S 2013 *Science* **340** 1545–8
[14] Banerji A, Singh R P, Banerjee D and Bandyopadhyay A 2016 *Phys. Rev.* A **94** 053838
[15] Huang K, Liu H, Restuccia S, Mehmood M Q, Mei S T, Giovannini D, Danner A, Padgett M J, Teng J H and Qiu C W 2018 *Light Sci. Appl.* **7** 17156
[16] Mondal P K, Deb B and Majumder S 2014 *Phys. Rev.* A **89** 063418
[17] Das B C, Bhattacharyya D and De S 2016 *Chem. Phys. Lett.* **644** 212–8
[18] Qu K, Jia Q and Fisch N J 2017 *Phys. Rev.* E **96** 053207
[19] Jack B, Leach J, Romero J, Franke-Arnold S, Ritsch-Marte M, Barnett S M and Padgett M J 2009 *Phys. Rev. Lett.* **103** 083602
[20] Yue F, Wen D, Xin J, Gerardot B D, Li J and Chen X 2016 *ACS Photon.* **3** 1558–63
[21] Mei S *et al* 2016 *Nanoscale* **8** 2227–33
[22] Wei B-Y, Chen P, Ge S-J, Duan W, Hu W and Lu Y-Q 2016 *Appl. Phys. Lett.* **109** 121105
[23] Fang Z X, Chen Y, Ren Y X, Gong L, Lu R D, Zhang A Q, Zhao H Z and Wang P 2018 *Opt. Express* **26** 7324–35
[24] Ostrovsky A S, Rickenstorffparrao C and Arrizon V 2013 *Opt. Lett.* **38** 534–6
[25] Porfirev A and Kuchmizhak A 2018 *Appl. Phys. Lett.* **113** 171105
[26] Chen Y, Fang Z X, Ren Y X, Gong L and Lu R D 2015 *Appl. Opt.* **54** 8030–5
[27] Li P, Zhang Y, Liu S, Ma C, Han L, Cheng H and Zhao J 2016 *Opt. Lett.* **41** 2205–8
[28] Chen M, Mazilu M, Arita Y, Wright E M and Dholakia K 2013 *Opt. Lett.* **38** 4919–22
[29] Reddy S G, Vaity C P P, Aadhi A, Prabhakar S and Singh R P 2016 *J. Opt.* **18** 055602
[30] Kovalev A, Kotlyar V and Porfirev A 2017 *Appl. Phys. Lett.* **110** 261102
[31] Abramochkin E and Volostnikov V 1996 *Opt. Commun.* **125** 302–23
[32] Rodrigo J A, Alieva T, Abramochkin E and Castro I 2013 *Opt. Express* **21** 20544–55

[33] Kotlyar V V, Kovalev A A and Porfirev A P 2018 *Optik* **156** 49–59
[34] Vaity P and Rusch L 2015 *Opt. Lett.* **40** 597–600
[35] Mirhosseini M, Maganaloaiza O S, Chen C, Rodenburg B, Malik M and Boyd R W 2013 *Opt. Express* **21** 30196–203
[36] Fang Z X, Zhao H Z, Chen Y, Lu R D, He L Q and Wang P 2018 *Sci. Rep.* **8** 8593
[37] Naylor D 2003 *Int. J. Heat Fluid Flow* **24** 345–55
[38] Rodrigo J A and Alieva T 2016 *Sci. Rep.* **6** 35341
[39] Jenness N J, Hill R T, Hucknall A, Chilkoti A and Clark R L 2010 *Opt. Express* **18** 11754–62